Energy Equip. Sys./ Vol. 12/No. 1/March 2024/ 1-10

ENERGY EQUIPSYS

Energy Equipment and Systems

http://energyequipsys.ut.ac.ir
www.energyequipsys.com

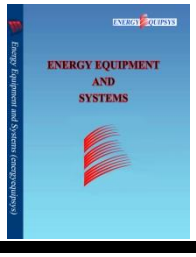

Interaction between two spheroidal drops in Couette flow: impact of initial offset and deformability

Authors

Parisa Armandoost[a]
Morteza Bayareh[a*]
Afshin Ahmadi Nadooshan[a]

[a]Department of Mechanical Engineering, Shahrekord University, Shahrekord, Iran

ABSTRACT

The collision of two spheroidal drops in a shear flow is simulated in this paper using the finite difference/front tracking method. The influences of deformability, initial offset, and the size of drops on their collision dynamics are assessed. It is demonstrated that the non-dimensional relative trajectory of a pair of drops, $\Delta z/R$, is enhanced gradually as they approach and then, gains a maximum value and finally, reaches a new constant value after separation. An enhancement in the capillary number results in an increase in the deformation of the drops. The deformation and the time required for the collision of two drops are reduced as their initial offset is enhanced. It is revealed that as the ratio of major diameter to minor diameter of spheroidal drops is intensified, their deformation is enhanced.

Article history:
Received : 17 December 2022
Accepted : 11 August 2023

Keywords: Front Tracking, Spheroidal Drops, Interaction, Couette Flow.

1. Introduction

Interaction between two deformable particles plays a crucial role in determining the behavior of emulsions. Besides, the assessment of the migration of a single deformable drop/bubble leads to the understanding of their collision dynamics [1]. The study of drop deformation and breakup was performed by Taylor [2] in 1932. Taylor's experiments revealed the existence of steady rounded and pointed drops, as well as bursting drops of the same type, depending on the viscosity ratio and the capillary number. In 1992, Unverdi and Tryggvason [3] describes a front-tracking method to simulate unsteady multi-phase flows in which a sharp interface or a front separates incompressible fluid of different densities and viscosities. In this method, a conservative finite difference is employed for the approximation on a stationary grid and the interface is explicitly represented by a separate, unstructured grid that moves through the stationary grid. The effect of surfactants on the deformation of drops and bubbles was examined by Lee and Pozrikidis [4]. Their results demonstrated the effect of the surfactant on the drop deformation and structure of the flow and showed the possibility of interface immobilization due to the Marangoni effect even for moderate variations in the surfactant concentration. Loewenberg and Hinch [5] evaluated the interaction between a

* Corresponding author: Bayareh, Morteza
Department of Mechanical Engineering, Shahrekord University, Shahrekord, Iran
Email: m.bayareh@sku.ac.ir

pair of deformable drops in a simple shear flow by using a boundary integral formulation. They observed that the interactions do not promote the breakup of the drops. Moreover, the lubrication gap that separates the two drops can decrease rapidly in the extensional quadrant of the flow for certain viscosity ratios. Guido and Simone [6] studied the collision of two equal-sized drops which were immersed in an immiscible liquid phase undergoing a shear flow for a range of the capillary number. They found the distance between the drop centers along the velocity gradient direction is enhanced irreversibly after the collision. They also indicated the evolution of drop shape during the collision basis on a deformation parameter and the angle between the drop major axis and the velocity gradient direction. Shardt et al. [7] simulated the collision of two equal-sized droplets in simple shear flow by using the lattice Boltzmann method and determined the critical capillary number for coalescence. It was observed that the critical capillary number is decreased when the droplet size is increased. Also, they demonstrated that the Peclet number affects the collision dynamics of drops. Lac and Bissel [8] assessed the collision of two identical capsules which consist of a viscous liquid drop and an elastic membrane in simple shear flow by using a boundary integral formulation. They showed that after the capsules cross each other, the hydrodynamic interaction is specified by an irreversible cross-flow displacement. It was shown the capsules exhibit negative deflections which displace them to closer streamlines. Bayareh and Mortazavi [9] simulated the three-dimensional migration of a spherical drop in a simple shear flow and revealed that a drop migrates towards the center of the channel and the migration rate depends on the surface tension and the fluid velocity. The duration of the migration increases by enhancing the Weber number and reducing the Reynolds number. Bayareh and Mortazavi [10] considered the collision of two equal-sized drops in an immiscible phase undergoing a shear flow over a range of the viscosity ratio by using the finite difference/front tracking method. They revealed that the distance between drop centers along the velocity gradient direction, i.e. Δz, is enhanced after the collision and reaches a new constant value after separation. Also, Δz is increased during the interaction by enhancing the initial offset. Based on their investigations, it was shown that the maximum deformation is the same for equal drop sizes and when the size of drops is reduced, the deformation is decreased. Moreover, the drops rotate more quickly when the initial offset increases. They investigated the effect of the viscosity ratio and showed that when the viscosity ratio is intensified, the rotation of drops is more slowly and the point of separation of drops occurs with delay. Magna and Stone [11] investigated the time-dependent interactions between two buoyancy-driven deformable drops at low Reynolds numbers. The interaction between two horizontally offset drops was studied experimentally and boundary integral simulations. It was shown that the axisymmetric drop configuration is stable for sufficiently deformable drops. Moreover, three modes for film drainage between drops were introduced as rapid drainage, uniform drainage, and dimple formation. Yoon et al. [12] studied the coalescence of two equal-sized deformable drops in an axisymmetric flow by using the boundary integral method. It was observed that the collision of drops exhibits two distinctively different regimes. At low capillary numbers, the interface of thin film between the colliding drops remains almost spherical up to the point of film rupture, and the drainage time is relatively short because a steep pressure gradient is formed at the center of the film. At high capillary numbers, the film becomes dimpled at an early stage of the collision process and the rate of the film drainage significantly slows down after the dimple is completely formed. Chen et al. [13] investigated experimentally the effect of confinement on the coalescence of Newtonian droplets in simple shear flow. The experimental result identified parameter ranges over which the transition from coalescence to non-coalescence occurs.

The interaction between drops/bubbles in various Newtonian and non-Newtonian fluids has been also considered in recent years. Mirsandi et al. [14] analyzed the collision between two bubbles in a viscoelastic liquid and demonstrated that the bubbles repel at low Reynolds numbers and attract each other at moderate and high Reynolds numbers. Balla et al. [15] considered the attractive and repulsive treatments of two spherical bubbles ascending

side-by-side in a non-isothermal fluid and revealed that they keep their spherical shape when the Weber number is low. Javier et al. [16] evaluated the interaction between two bubbles created due to an underwater explosive numerically and experimentally and found that the amount of impulse is dependent on the location and symmetry of collapse. Zhang et al. [17] calculated the interaction force between a particle and an air bubble or a water droplet and showed that strong and weak adhesion occurs between particle/droplet and particle/bubble, respectively. Yan et al. [18] examined the bubbles/droplets attachment in oily water. It was demonstrated that their size enhancement augments the spreading time.

Even though the interaction of spherical drops/bubbles has been evaluated numerically and experimentally, the collision of non-spherical deformable particles has not been considered. Experimental investigations have revealed that the shape of liquid drops can be changed during the interaction with the carrier phase [19, 20]. Numerical studies have demonstrated that the surface of drops is related to the local mean curvature due to the application of non-uniform heat fluxes on their surface [21, 22]. It can be concluded that the non-uniform distribution of heat fluxes on their surface leads to the non-uniform distribution of temperature on spheroidal drops during the heating and evaporation processes [23]. Some investigators analyzed the Stokes and turbulence flow around prolate spheroids [24], the evaporation of spheroidal drops [25], the interaction between a spheroidal drop and a wall [26], the impact of deviation from the spherical shape of drops on mass transport equation [27], the motion of a spheroidal drop suspended in a fluid [28], and collision between two spheroidal particles [29]. The understanding of this phenomenon is crucial because there are many deformable particles with non-spherical shapes like spheroidal ones. In this study, the collision of two spheroidal drops is simulated using the finite-difference/front tracking method to evaluate the impact of deformability (capillary number), their initial offset, and initial size on the collision dynamics (Fig. 1).

2. Governing equations

The Navier-Stokes equations in conservative form govern the interaction between two deformable drops in a simple shear flow [30]:

$$\frac{\partial \rho \mathbf{u}}{\partial t} + \nabla.\rho\mathbf{u} = -\nabla P + \rho\mathbf{f} + \nabla.\mu\left(\nabla\mathbf{u} + \nabla^{T}\mathbf{u}\right) + \int \sigma k'\mathbf{n}'\delta^{\beta}\left(x - x'\right)ds' \quad (1)$$

This equation is valid for the entire flow field, even if the density field, ρ, and the viscosity field, μ, change discontinuously. Here, **u** is the velocity vector, **P** is the pressure and **f** is the body force. δ^{β} is a function that refers to the dimensions of flows. k′ is the curvature of flows, **n** is the unit vector normal to the front, **x** shows the Eulerian coordinate, and **x′** indicates the coordinate of a point on the drop, i.e. Lagrangian coordinate.

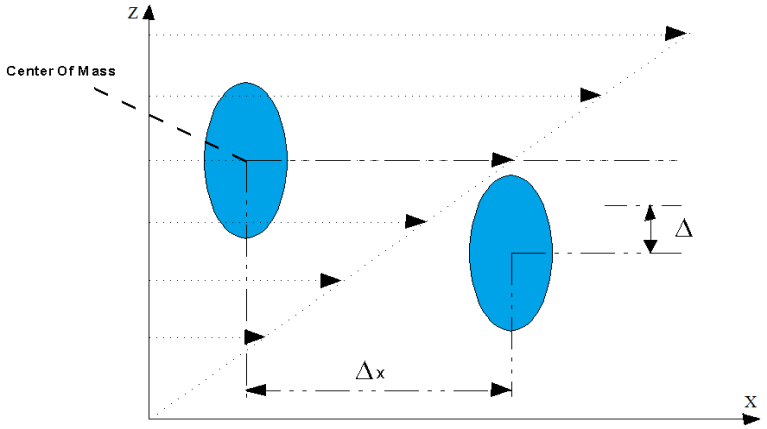

Fig. 1. Schematic of the interaction between a pair of deformable drops in shear flow (Offset = Δ/R, where R is the equivalent radius of a spherical drop with the same surface area).

Mass conservation is also given as follows:

$$\frac{\partial \rho}{\partial t} + \nabla . \rho \mathbf{u} = 0 \tag{2}$$

The density is constant while the flow is incompressible, therefore:

$$\frac{D\rho}{Dt} = 0 \tag{3}$$

Thus, the continuity equation reduces to

$$\nabla . \mathbf{u} = 0 \tag{4}$$

Moreover, the viscosity is considered constant:

$$\frac{D\mu}{Dt} = 0 \tag{5}$$

The collision of drops in simple shear flow is affected by several non-dimensional parameters. The first dimensionless parameter is the bulk Reynolds number which is defined as

$$Re_b = \frac{\rho_o G H^2}{\mu_o} \tag{6}$$

where H is the height of the channel and G is defined as the shear ratio is given by

$$G = \frac{u_t - u_b}{H} \tag{7}$$

where u_t and u_b are the velocities of the top and bottom walls, respectively.

The second dimensionless parameter is the capillary number, which is given by

$$Ca = \frac{\mu_o G d_e}{\sigma} \tag{8}$$

Here, d_e is the diameter of a spherical that has equal volume with the volume of an ellipsoidal drop and σ is the surface tension coefficient.

The density ratio is also defined as

$$\eta = \frac{\rho_i}{\rho_o} \tag{9}$$

where ρ_i and ρ_o are the density of drop and ambient fluid, respectively.

The viscosity ratio is calculated using

$$\lambda = \frac{\mu_i}{\mu_o} \tag{10}$$

where μ_i and μ_o are the viscosity of drop and ambient fluid, respectively.

3. Numerical method

The multiphase flow problems are simulated using various methods, including the MAC method, which uses marked particles to identify each fluid, the volume of fluid (VOF) method, which utilizes a mark function, Lagrangian methods that follow the fluid grid, the front tracking method, which a separate front marks the interface, but a stationary grid is employed for the fluid of each phase (Fig. 2).

The Front-tracking method is used to simulate the interaction of two drops in simple shear flow which is a combination of a stationary and Lagrangian grid.

The Navier-Stokes equations are solved on a fixed grid and the surface tension is calculated on the boundary of the front. The surface quantity, Q_f, is expressed in units per area, and the grid value, Q_g, should be given in terms of units per volume; hence

$$\int_{\Delta s} \varnothing_f(s)\,ds = \int_{\Delta v} \varnothing_g(\mathbf{x})\,dv \tag{11}$$

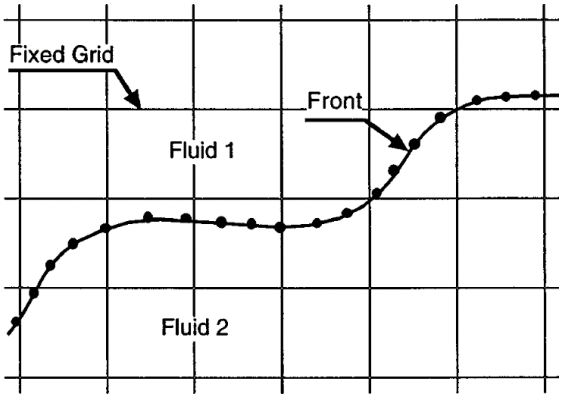

Fig. 2. The position of the Lagrangian grid on a stationary Eulerian grid for multiphase flows.

The force that is related to surface tension on each element of the front is calculated by

$$\delta \mathbf{F}_\sigma = \int_{\Delta s} \sigma k \mathbf{n} d_s \tag{12}$$

The average surface curvature can be written as

$$k\mathbf{n} = (\mathbf{n} \times \nabla) \times \mathbf{n} \tag{13}$$

Then, the force on each element's surface is calculated using

$$\mathbf{F}_\sigma = \sigma \int_{\delta A} k\mathbf{n}\, dA = \sigma \int_{\delta A} (\mathbf{n} \times \nabla) \times \mathbf{n}\, dA = \sigma \tilde{}_s\, \mathbf{t} \times \mathbf{n}\, ds \tag{14}$$

Here, **t** and **n** are the tangential and normal vectors to each element.

4. Results

4.1. Grid study and validation

To perform a grid study, the dimensionless amount of Δz is calculated for different grid resolutions of 32×32, 64×64, 128×128, and 256×256. It is found that the grid with 1282 nodes is sufficient for the simulations. Besides, for the verification of numerical simulations, the present results are compared with the experimental data of Guido and Simeone [6] (Fig. 3) who considered the collision between two spherical drops. In this figure, the amounts of Δz/R are plotted as a function of Δx/R for an initial offset of 0.4 and λ=1. It is observed that Δz enhances and reaches a maximum value after approaching and contacting drops with each other. After separation, it has a constant value.

4.2. Interaction between a pair of spheroidal drops

To simulate the collision between two spheroidal drops, their centers are not in a line initially. The center of the front drop is slightly lower than the middle of the line between the two drops and the center of the rear one is slightly higher than the middle of the mentioned line. This geometry is selected to recognize the physics of the collision. The difference in the distance between the centers of the drops results in the relative trajectory of the two drops along the x and z axes which are expressed in terms of the differences $\Delta z=z_2-z_1$ and $\Delta x=x_2-x_1$, where x_i and z_i are the center of mass coordinates of the ith drop. It should be pointed out that the difference between the y-coordinates of the two drop centers is zero. When two spheroidal drops collide with each other in simple shear flow, five modes can be determined: approach, collision, slide, tumbling, and separation. For instance, Fig. 4 demonstrates the sequences 1-5 when Ca = 0.2, offset = 2, and λ = η = 1.

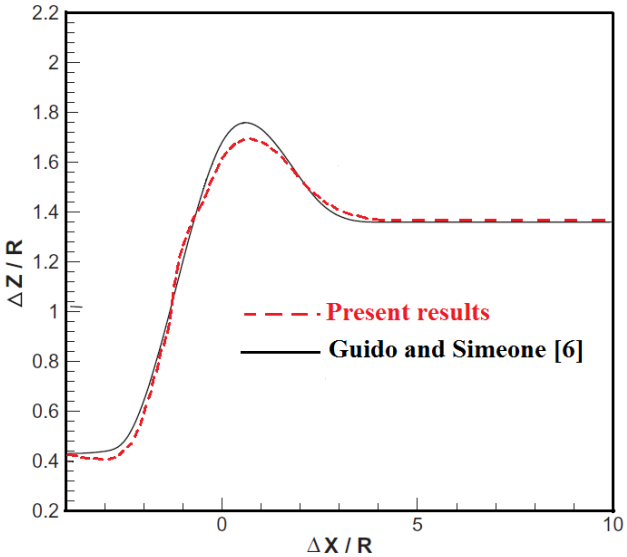

Fig. 3. The variations of Δz/R versus Δx/R for Ca = 0.13, Re_b=10, and λ = 0.25.

Fig. 4. Sequences (1-5) exhibiting the binary collision of drops in simple shear flow when Ca = 0.2, offset = 2, and $\lambda = \eta = 1$.

4.3. Effect of deformability

The deformability of drops can be evaluated by the capillary number. Figure 5 illustrates the values of $\Delta z/R$ as a function of dimensionless time for different capillary numbers during the approach, collision, and separation. As can be seen, $\Delta z/R$ is enhanced gradually as the droplets approach and then reaches a maximum value and finally, reaches a new constant value after separation. Armandoost et al. [31] reported that the drop deformation is enhanced by increasing the capillary number or decreasing surface tension. Higher deformation leads to the drops becoming closer to each other and their centers are placed at a closer distance during the collision process.

Figure 6 illustrates the deformations of the drops in the tumbling mode for different capillary numbers. The tumbling mode is one of the pressure stages of the collision between two drops. The capillary number expresses the ratio of viscosity to surface tension. Therefore, the deformation of the drops increases with the capillary number.

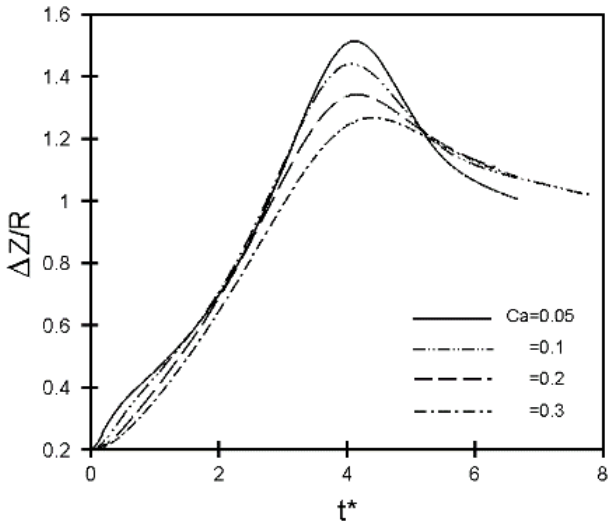

Fig. 5. Relative trajectory of two interacting drops in shear flow for different capillary numbers when $Re_b = 10$ and $\lambda = \eta = 1$.

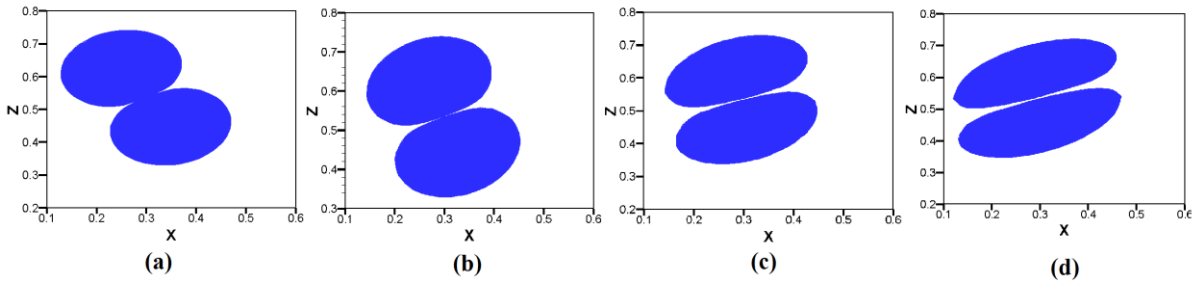

Fig. 6. Tumbling mode of two deformable drops in simple shear flow when $Re_b = 10$, $\eta = \lambda = 1$, and (a) Ca = 0.05, (b) Ca = 0.1, (c) Ca = 0.2, and (d) Ca=0.3.

Figure 7 demonstrates the sequences (1-5) of the collision of two drops, indicating that the deformation of drops gradually increases during the approach stage and reaches a maximum value (point 3). After that, it reaches a minimum value (point 4) and a second maximum value (point 5), which is smaller than the first maximum one. Finally, it reaches a constant value.

The relative velocity between the centers of the drops in the flow direction (ΔV_x) in terms of $\Delta x/R$ is shown in Fig. 8a. When the drops start to collide, ΔV_x increases rapidly, showing their acceleration during tumbling mode. It can also be seen that the final value of ΔV_x is greater than its initial value due to the increase in their lateral distance. The negative value of ΔV_x is due to the small initial distance between the centers of the drops in the x-direction. Due to the presence of the front drop, the trailing drop cannot move under the influence of the shear flow, and only the front drop can move in the flow direction. When the drops are deformed, the rear one reaches a necessary initial acceleration and ΔV_x becomes positive. For this reason, the distance between the centers of the drops increases. Figure 8b depicts the relative velocity between the centers of the droplets in the direction of the velocity gradient (ΔVz) in terms of $\Delta x/R$. The value of ΔVz before and after the collision is zero. It is positive during the tumbling mode and negative when they are separated.

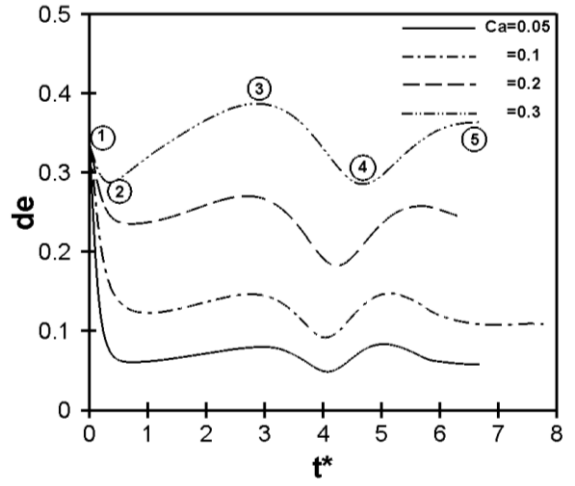

Fig. 7. Deformation of two interacting drops as a function of dimensionless time when $\lambda = \eta = 1$ and $Re_b = 10$ for different capillary numbers.

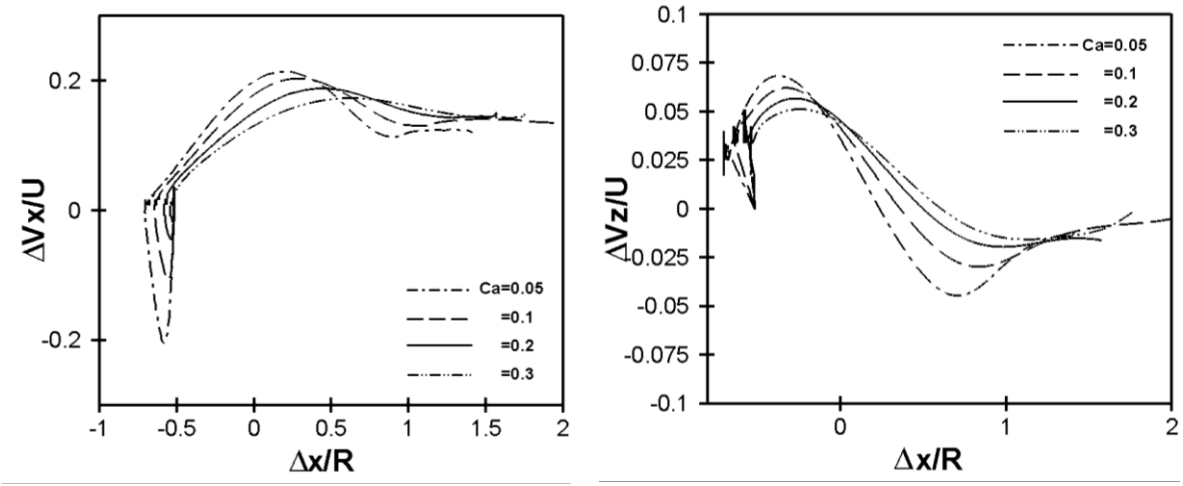

(a) (b)

Fig. 8. Dimensionless amounts of (a) ΔV_x and (b) ΔVz versus $\Delta x/R$ for $Re_b = 10$, $\lambda = \eta = 1$, and different capillary numbers.

4.4. Effect of initial offset and size of drops

The initial offset is defined as the ratio of the half-shortest distance between the centers of the drops (Δ) to the equivalent radius of the undeformed drops (Fig. 1). Fig. 9a illustrates the non-dimensional lateral distance between two drops, i.e. ΔVz, in terms of Δx/R for different values of the initial offset. The final value of Δz/R for offsets 4.2, 5.5, and 5.7 is equal to 0.55, 0.57, and 0.61, respectively. These values are greater than the initial value of Δz/R. In other words, if the drops collide with each other again, they will gain a larger lateral distance, indicating that this phenomenon is irreversible. Fig. 9b shows the variations of deformation versus dimensionless time. It can be seen that as the initial offset is reduced, the deformation and the time required for the droplets to approach each other are enhanced. Since the difference between the values of the initial offset is small, the maximum deformation is approximately the same.

To evaluate the impact of the size of drops on their collision dynamics, the amount of deformation is calculated for two different ratios of L/B in Fig. 9c when the initial offset is 5.7. As can be seen, the larger the value of L/B, the larger the deformation.

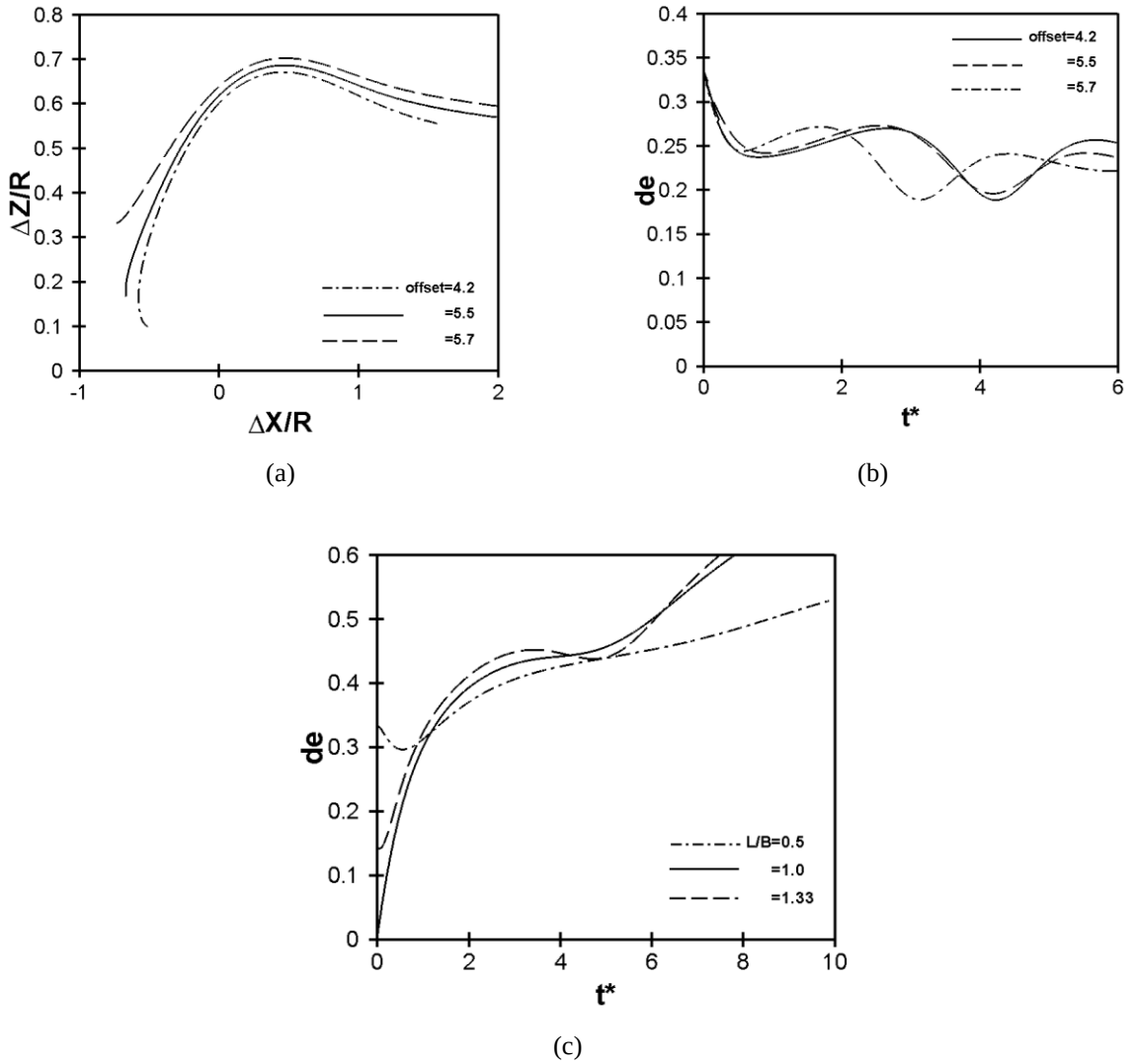

Fig. 9. (a) Dimensionless amounts of Δz versus Δx/R, and (b) deformation in terms of non-dimensional time for Re_b = 10, λ = η = 1, and different amounts of initial offset. (c) The deformation versus dimensionless time for Re_b = 10, Ca = 0. 075, λ = η = 1, and different sizes of drops.

5. Conclusions

Simulation of the binary collision of spherical/non-spherical drops in shear flow is very important. In the present paper, the interaction between two spheroidal drops is simulated using the finite difference/front tracking method. It is found that the relative trajectory of the center of drops is enhanced due to their collision. Also, the deformation of the droplets causes they do not merge. The interaction of two spheroidal drops involves three stages, like spherical ones: approach, collision, and separation. The results demonstrate that the relative trajectory of the drops is enhanced gradually as they approach, then reaches a maximum value, and then reaches a new constant value after separation. This lateral distance is reduced with the capillary number. An increment in the capillary number causes an enhancement in the deformation of the drops. When the drops collide, their relative velocity in the flow direction is enhanced rapidly, indicating that they accelerate during the tumbling state. As the initial offset becomes larger, the drops rotate faster and the time required for collision is reduced. Finally, it is demonstrated that the larger the value of L/B, the larger the deformation.

References

[1] Bayareh, M., Mortazavi, S., Effect of density ratio on the hydrodynamic interaction between two drops in simple shear flow, Iranian Journal of Science and Technology (2011) 35: 121-132.

[2] Taylor, G.I., The formation of emulsions in definable fields of flow. Proceedings of the Royal Society of London. Series A, containing papers of a mathematical and physical character (1934) 146: 501-523.

[3] Unverdi, S.O., Tryggvason, G., A front-tracking method for viscous, incompressible, multi-fluid flows. Journal of computational physics (1992) 100(1): 25-37.

[4] Li, X., Charles, R., Pozrikidis, C., Simple shear flow of suspensions of liquid drops. Journal of Fluid Mechanics (1996) 320: 395-416.

[5] Loewenberg, M., Hinch, E., Collision of two deformable drops in shear flow. Journal of Fluid Mechanics (1997) 338: 299-315.

[6] Guido, S., Simeone, M., Binary collision of drops in simple shear flow by computer-assisted video optical microscopy. Journal of Fluid Mechanics (1998) 357: 1-20.

[7] Shardt, O., Derksen, J., Mitra, S.K., Simulations of droplet coalescence in simple shear flow. Langmuir (2013) 29(21): 6201-6212.

[8] Lac, E., Barthès-Biesel, D., Pairwise interaction of capsules in simple shear flow: Three-dimensional effects. Physics of Fluids (2008) 20(4): 040801.

[9] Bayareh, M., Mortazavi, S., Equilibrium position of a buoyant drop in Couette and Poiseuille flows at finite Reynolds numbers, Journal of Mechanics (2013) 33:53-58.

[10] Bayareh, M., Mortazavi, S., Binary collision of drops in simple shear flow at finite Reynolds numbers: Geometry and viscosity ratio effects, Advances in Engineering Software (2011) 42: 604-611.

[11] Manga, M., Stone, H.A., Buoyancy-driven interactions between two deformable viscous drops. Journal of Fluid Mechanics (1993) 256: 647-683.

[12] Yoon, Y., et al., Viscosity ratio effects on the coalescence of two equal-sized drops in a two-dimensional linear flow. Journal of Fluid Mechanics (2005) 525: 355-379.

[13] Chen, D., Cardinaels, R., Moldenaers, P., Effect of confinement on droplet coalescence in shear flow. Langmuir (2009) 25(22): 12885-12893.

[14] Mirsandi, H., Kong, G., Buist, K.A., Baltussen, M.W., Peters, E.A.J.F., Kuipers, J.A.M., Numerical study on the interaction of two bubbles rising side-by-side in viscous liquids. Chemical Engineering Journal (2021) 410: 128257.

[15] Balla, M., Tripathi, M.K., Matar, O.K., Sahu, K.C., Interaction of two non-coalescing bubbles rising in a non-isothermal self-rewetting fluid. European Journal of Mechanics - B/Fluids (2021) 87: 103–112.

[16] Javier, C., Galuska, M., Papa, M., LeBlanc, J., Matos, H., Shukla, A., Underwater explosive bubble interaction with an adjacent submerged structure.

Journal of Fluids and Structures (2021) 100: 103189.

[17] Zhang, Y., Xing, Y., Ding, S., Cao, Y., Gui, X., New method to measure interaction force between particle and air bubble/water droplet using a micro-Newton mechanics testing instrument, Powder Technology (2020), doi:10.1016/j.powtec.2020.06.049

[18] Yan, S., Yang, X., Bai, Z., Xu, X., Wang, H., Drop attachment behavior of oil droplet-gas bubble interactions during flotation. Chemical Engineering Science (2020), doi:10.1016/j.ces.2020.115740

[19] Mashayek, F., Dynamics of evaporating drops. Part I: formulation and evaporation model. International Journal of Heat and Mass Transfer (2001) 44(8): 1517–1526.

[20] Loth, E., Quasi-steady shape and drag of deformable bubbles and drops. International Journal of Multiphase Flow (2008) 34(6): 523–546.

[21] Hase, M., Weigand, B., Transient heat transfer of deforming droplets at high Reynolds numbers. International Journal of Numerical Methods for Heat & Fluid Flow (2004) 14(1): 85–97.

[22] Schlottke, J., Weigand, B., Direct numerical simulation of evaporating droplets. Journal of Computational Physics (2008) 227(10): 5215–5237.

[23] Zubkov, V.S., Cossali, G. E., Tonini, S., Rybdylova, O., Crua, C., Heikal, M., Sazhin, S.S., Mathematical modelling of heating and evaporation of a spheroidal droplet. International Journal of Heat and Mass Transfer (2017) 108: 2181–2190.

[24] Sanjeevi, S.K.P., Dietiker, J.F., Padding, J.T., Accurate hydrodynamic force and torque correlations for prolate spheroids from Stokes regime to high Reynolds numbers, Chemical Engineering Journal (2022) 444: 136325.

[25] Tonini, S., Cossali, G.E., An analytical model for the evaporation of multi-component spheroidal drops based on Stefan–Maxwell equations, International Journal of Thermal Sciences (2022) 171: 107223.

[26] Cui, Y., Wang, Y., Jin, Z., Hu, R., Meng, K., Shan, B., Liu, Y.,Analysis of multiple successive collisions between a prolate spheroidal particle and a plane wall, Powder Technology (2023) 118878.

[27] Tonini, S., Cossali, G.E., An exact solution of the mass transport equations for spheroidal evaporating drops, International Journal of Heat and Mass Transfer (2013) 60: 236-240.

[28] Zabarankin, M., Analytical Solution for Spheroidal Drop under Axisymmetric Linearized Boundary Conditions, SIAM Journal on Applied Mathematics (2016) 76(4): 1606–1632.

[29] Zhu, C., Yu, Z., Pan, D., Shao, X., Interface-resolved direct numerical simulations of the interactions between spheroidal particles and upward vertical turbulent channel flows, Journal of Fluid Mechanics (2020) 891.

[30] Bayareh, M., Mortazavi, S., Three-dimensional numerical simulation of drops suspended in simple shear flow at finite Reynolds numbers. International Journal of Multiphase Flow (2011) 37(10): 1315-1330.

[31]Armandoost, P., Bayareh, M., Ahamdi Nadooshan, A., Study of the motion of a spheroidal drop in a linear shear flow. Journal of Mechanical Science and Technology (2018) 32(5): 2059-2067.